

THE EARLY EVOLUTION OF MASSIVE STARS: RADIO RECOMBINATION LINE SPECTRA

ERIC KETO AND QIZHOU ZHANG

Harvard-Smithsonian Center for Astrophysics, 60 Garden Street, Cambridge, MA 02138

AND

STANLEY KURTZ

CRyA, Universidad Nacional Autónoma de México, Apartado Postal 3-72, 58090 Morelia, Michoacán, Mexico

Received 2007 March 17; accepted 2007 August 11

ABSTRACT

Velocity shifts and differential broadening of radio recombination lines are used to estimate the densities and velocities of the ionized gas in several hypercompact and ultracompact H II regions. These small H II regions are thought to be at their earliest evolutionary phase and associated with the youngest massive stars. The observations suggest that these H II regions are characterized by high densities, supersonic flows, and steep density gradients, consistent with accretion and outflows that would be associated with the formation of massive stars.

Subject headings: H II regions — stars: early-type — stars: formation

1. INTRODUCTION

Massive star-forming regions are marked by small (≤ 0.1 pc) H II regions (Gaume et al. 1995a; DePree et al. 1997, 1998, 2000, 2004, 2005; Tieftrunk et al. 1997; Wilson et al. 2003) that are characteristically different from many of the few thousand ultracompact H II (UCH II) regions scattered throughout the galaxy (Wood & Churchwell 1989; Kurtz et al. 1994; Walsh et al. 1998; Giveon et al. 2005a, 2005b). First, these very small H II regions have electron densities that are higher ($n_e \geq 10^5 \text{ cm}^{-3}$) than those of UCH II regions ($n_e \sim 10^4 \text{ cm}^{-3}$; Kurtz 2000; Kurtz & Franco 2002; Pratap et al. 1992). It is unclear how high the densities might be, because the density cannot be reliably determined from the radio continuum if the gas is optically thick. Second, when observed at centimeter wavelengths, these small H II regions often show very broad radio recombination line (RRL) widths, more than 3 or 4 times the thermal line width (Altenhoff et al. 1981; Zijlstra et al. 1990; Afflerbach et al. 1994; DePree et al. 1994, 1995, 1996, 1997; Gaume et al. 1995b; Keto et al. 1995; Johnson et al. 1998; Jaffe & Martín-Pintado 1999; Keto 2002; Sewilo et al. 2004; Keto & Wood 2006). Not all the small H II regions have this property, but those that do are sometimes referred to as broad recombination line objects. The breadth of the RRLs could be caused by a combination of electron impact (pressure) broadening associated with high gas density plus broadening caused by spatially unresolved gas motions. However, the relative contributions of broadening due to gas pressure and gas motions are not known. Third, these H II regions often have continuum spectral energy distributions (SEDs) that are roughly linear with frequency over decades in wavelength from the centimeter to the submillimeter (Hofner et al. 1996; Franco et al. 2000; Testi et al. 2000; Beuther et al. 2004; Ignace & Churchwell 2004). The underlying cause of this scaling is not known, although spatially unresolved density variations are a possibility.

These small and dense H II regions are sometimes referred to as hypercompact H II (HCH II) regions. While the term hypercompact implies a size smaller than ultracompact, the three properties of high electron densities, broad recombination lines, and linear SEDs are also seen in some UCH II regions (~ 0.1 pc). The common characteristic might be that they both are young and at the earliest evolutionary stage, but the unusual UCH II regions might contain more or brighter stars than their smaller HCH II counterparts.

That the HCH II and unusual UCH II regions represent some of our best sources of information on the processes in the formation of massive stars motivates our understanding of their special properties.

In this paper we report on multifrequency RRL observations that address the origin of the three properties of the small H II regions and the processes of massive star formation. We compare the widths of RRLs observed at different frequencies to estimate the gas density and the range of velocities in gas motions within the H II regions. These estimates suggest that the HCH II regions are characterized by high gas densities $n > 10^6 \text{ cm}^{-3}$, steep density gradients $n \propto r^\alpha$ with $\alpha = -1.5$ to -2.5 , and supersonic velocities.

2. OBSERVATIONS

We selected a few well-studied, very bright, very small H II regions that previous observations suggest have one or more of the three properties of the small H II regions. For each source we have one observation of the H30 α line made with the Submillimeter Array (SMA) and one or more observations of centimeter wavelength RRLs made with the National Radio Astronomy Observatory Very Large Array (VLA).¹

The SMA observations of the H30 α line (231.900959 GHz) in the H II regions G10.6–0.04, NGC 7538-IRS1, W51e2, and G28.20–0.04 were made in 2005 September with a spectral resolution of 0.83 km s^{-1} , a bandwidth of 2 GHz, and an angular resolution of $1.0''$. Observations of G45.07+0.14 were made in 2005 October with an angular resolution of $0.4''$. The noise level obtained in each observation was $60 \text{ mJy beam}^{-1} \text{ channel}^{-1}$. Analysis of the data indicated that some of the baselines were not well defined; hence, the positions and flux densities of the sources are uncertain. The standard deviation of the flux of 3C 454.4, measured once for each observation, is 39% of the average measured value (Table 1). If we exclude the low measurement of 3C 454.4 corresponding to the G45.07+0.14 data, then the standard deviation falls to 14% of the average. Our positions from the SMA agree with those of the VLA to better than the angular

¹ The National Radio Astronomy Observatory is a facility of the National Science Foundation operated under cooperative agreement by Associated Universities, Inc.

TABLE 1
CALIBRATION OF MILLIMETER OBSERVATIONS

SOURCE	BAND	FLUX		BANDPASS		GAIN	
		Calibrator	Flux (Jy)	Calibrator	Flux (Jy)	Calibrator	Flux (Jy)
G10.60–0.4.....	SMA	Ceres	0.7	3C 454.3	16.8	PKS 1911-201	1.4
G28.20–0.04 N.....	SMA	3C 454.3	14.3	PKS 1911-201	1.8
G45.07+00.14.....	SMA	3C 454.3	4.6	PKS 2025+337	0.5
W51e2.....	SMA	Ceres	0.7	3C 454.3	16.0	PKS 2025+337	0.8
NGC 7538-IRS1.....	SMA	Ceres	0.5	3C 454.3	11.9	PKS 2202+422	3.0

NOTE.—Flux densities derived assuming a flux density for Uranus of 36.6 Jy.

resolution. The H II regions are unresolved by the SMA observations, and hence, the widths of their spectral lines are unaffected by baseline errors. The SMA data were processed in the SMA data reduction package MIR and in MIRIAD.

Most of the VLA observations were made in 2003 and 2005. We reprocessed observations of the H76 α line in G45.07+0.14 (Garay et al. 1986) from the VLA archives. The observations of the H66 α line in G10.6–0.4 were previously reported in Keto (2002). The other observations have not previously been published. Details of the observations are presented in Table 2. The VLA data were processed in AIPS; calibration data are given in Table 3. The recombination line spectra are shown in Figures 1–5, and the line widths and velocities are given in Table 4.

3. GAS VELOCITIES, PRESSURE BROADENING, AND ELECTRON DENSITIES

Radio recombination lines in H II regions are broadened by three contributions: thermal broadening, dynamical broadening due to spatially unresolved motions including both ordered flows and turbulence, and pressure broadening due to high electron densities. We seek to estimate the separate contributions of each of the three broadening mechanisms by comparing the widths of RRL observed at different frequencies. This is possible because the width due to thermal and dynamical broadening is independent of frequency, while the width due to pressure broadening decreases with frequency as $\Delta\nu \sim \nu^{-4}$ (Brocklehurst & Seaton 1972; Griem 1974). Since the dynamical broadening is proportional to the range of velocities in the gas while the pressure broadening is proportional to the gas density, from a pair of RRL

observations we can estimate the velocities and densities in the ionized gas.

We determine the contributions of each of the three broadening mechanisms as follows. We assume that the dynamical broadening, $\Delta\nu_d$, and the thermal broadening, $\Delta\nu_t$, combine in quadrature,

$$\Delta\nu_G = \sqrt{\Delta\nu_d^2 + \Delta\nu_t^2}. \quad (1)$$

This width due to gas motions, both thermal and spatially unresolved ordered flows and turbulence, combines with the Lorentzian width due to pressure broadening, $\Delta\nu_L$, to produce a Voigt profile with width, $\Delta\nu_V$. We approximate the width of the Voigt profile by an algebraic expression (Olivero & Longbothum 1977; eq. [2.72] in Gordon & Soroichenko 2002),

$$\Delta\nu_V = 0.5343\Delta\nu_L + [\Delta\nu_G^2 + (0.4657\Delta\nu_L)^2]^{1/2}, \quad (2)$$

where $\Delta\nu_V$ is the full width at half-maximum (FWHM) of the Voigt profile, $\Delta\nu_L$ the FWHM of the Lorentzian, and $\Delta\nu_G$ the FWHM of the Gaussian. Because of the rapid decrease in pressure broadening with frequency, the width of an RRL at a high enough frequency must be due solely to thermal broadening and spatially unresolved gas motions; therefore, $\Delta\nu_G$ in equation (2) is given by the observed width of our highest frequency RRL, H30 α . Any increased width observed in a lower frequency line must be due to pressure broadening, because the width $\Delta\nu_G$ is independent of frequency. We can then calculate the width due to pressure broadening, $\Delta\nu_L$, by solving the quadratic equation (2)

TABLE 2
VLA OBSERVATIONS

Source	R.A.	Decl.	Line	Frequency (GHz)	Spectral Resolution (km s ⁻¹)	Bandwidth Channel	Angular Resolution (arcsec)	Sensitivity ^a (mJy)	Date Observed
G10.6–0.4.....	18 10 28.7	–19 55 49	H92 α	8.309383	1.76	64	1.5 × 1.0	7	1989 Mar 17
			H66 α ^b	22.36417	2.62	64	1.7 × 1.0	9	1988 May 23
			H53 α	42.95197	1.36	64	1.5 × 1.3	3.0	2003 Feb 03
G28.20–0.04 N.....	18 42 58.17	–04 13 57.0	H53 α	42.95197	1.36	64	0.6 × 0.4	1.2	2005 Jun 24
			H53 α	42.95197	5.45	32	0.7 × 0.5	3.0	2005 Jun 28
G45.07+0.14 N.....	19 13 22.069	10 50 52.5	H76 α ^c	14.69000	15.95	16	0.6 × 0.6	10	1984 Jan 07
W51e2.....	19 23 43.913	14 30 14.7	H66 α	22.36417	2.62	64	0.3 × 0.2	1.6	2003 Feb 01
			H53 α	42.95197	1.36	64	0.5 × 0.4	0.9	2003 Feb 01
NGC 7538-IRS1.....	23 13 45.37	61 28 10.4	H53 α	42.95197	5.45	31	0.2 × 0.2	0.9	2005 Apr 17

NOTE.—Units of right ascension are hours, minutes, and seconds, and units of declination are degrees, arcminutes, and arcseconds.

^a Sensitivity over the full bandwidth rather than the sensitivity of an individual channel.

^b Data from the VLA archives. The original observation is reported in Keto 2002.

^c Data from the VLA archives. The original observation is reported in Garay et al. 1986.

TABLE 3
CALIBRATION OF CENTIMETER OBSERVATIONS

SOURCE	BAND	FLUX		BANDPASS		GAIN	
		Calibrator	Flux (Jy)	Calibrator	Flux (Jy)	Calibrator	Flux
G28.20–0.04 N	<i>Q</i>	3C 286	1.5	3C 273	24.2	PKS 1851+005	1.9
G45.07+00.14 N	<i>U</i>	3C 286	3.5	3C 454.3	7.5	PKS 1923+210	2.1
W51e2	<i>Q</i>	3C 286	1.5	3C 273	10.1	PKS 1923+210	2.6
W51e2	<i>K</i>	3C 286	2.5	3C 273	19.5	PKS 1923+210	3.1
NGC 7538-IRS1	<i>Q</i>	3C 48	0.5	3C 454.3	15.6	PKS 2250+558	0.8

with $\Delta\nu_V$ given by the observed width of the low-frequency line.

The range of gas velocities is estimated from equation (1). Assuming an ionized gas temperature of 8000 K, the dynamical widths are 15.3, 8.3, 27.1, 18.7, and 53.9 km s⁻¹ for G10.6–0.4, G28.20–0.04 N, G45.07+0.14, W51e2, and NGC 7538-IRS1, respectively.

The electron density may be estimated from the ratio of $\Delta\nu_L$ and $\Delta\nu_t$. For α ($\Delta N = 1$) transitions, the ratio of the Lorentzian width, $\Delta\nu_L$, resulting from pressure broadening, and the thermal width, $\Delta\nu_t$, is given by (Brocklehurst & Seaton 1972; Griem 1974; Keto et al. 1995)

$$\frac{\Delta\nu_L}{\Delta\nu_t} = 1.2 \left(\frac{n_e}{10^5} \right) \left(\frac{N}{92} \right)^7, \quad (3)$$

where n_e is the electron density in cm⁻³ and N is the principal quantum number.

As an example, we calculate the electron density in G10.6–0.4 from the H30 α and H92 α RRL observations as follows. We use the width of the H30 α line, 24.5 km s⁻¹ (Table 4), to estimate $\Delta\nu_G$ at the frequency of the H92 α line. Thus, $\Delta\nu_G = 0.678$ MHz. The measured width of the H92 α line is $\Delta\nu_V = 1.03$ MHz. From equation (2), the width due to pressure broadening is $\Delta\nu_L = 0.578$ MHz or 20.9 km s⁻¹. The thermal width, assuming a temperature of 8000 K, is $\Delta\nu_t = 1.43$ MHz or 19.1 km s⁻¹. The width due to gas motions is $\Delta\nu_d = (24.5^2 - 19.1^2)^{1/2} = 15.3$ km s⁻¹. The electron density from equation (3) is 9.1×10^4 cm⁻³. Similarly, from the observations of the other centimeter RRLs observed in G10.6–0.4, the electron den-

sities are 7.8×10^5 cm⁻³ from the H66 α line and 2.5×10^6 cm⁻³ from the H53 α line. Comparing these three RRLs, the electron density increases with the RRL frequency. If there is a density gradient in G10.6–0.4, this would suggest that the higher frequency lines are seeing deeper into the nebula where the electron densities are higher.

3.1. Uncertainties

We can check our approximation of negligible pressure broadening in the H30 α line from equation (3). For the H30 α line, this ratio is less than one as long as the density is less than 3×10^8 cm⁻³. Thus, our assumption of negligible pressure broadening in the H30 α line is valid up to this density.

The lines in our sample are not consistently Gaussian or Lorentzian probably because of nonisotropy in the gas motions. Nevertheless, we determine the line widths by fitting Gaussians because this provides a reasonable estimate if the observed profiles differ from a Gaussian most strongly in the wings and are similar in the core where the width is measured. An informal estimate of the possible error introduced by this method may be derived by fitting a Gaussian to a known Voigt profile. If the Gaussian and Lorentzian components of the Voigt are of equal FWHM, then a Gaussian fit overestimates the true FWHM of the Voigt by 10%.

We find that the procedure of using Gaussian line widths in equation (2) to estimate the pressure broadening is a more reliable method than some alternatives. For example, one could imagine fitting a Voigt profile directly to an observed low-frequency line to determine simultaneously both the Gaussian and Lorentzian components. However, we find this unreliable because the fitting

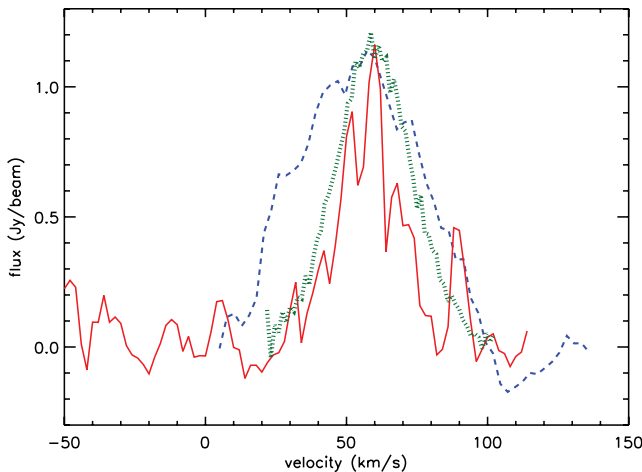


FIG. 1.—H66 α (dashed blue line), H53 α (dotted green line), and H30 α (solid red line) in W51e2. The flux densities of the H66 α line and the H53 α lines have been multiplied by 80 and 27, respectively.

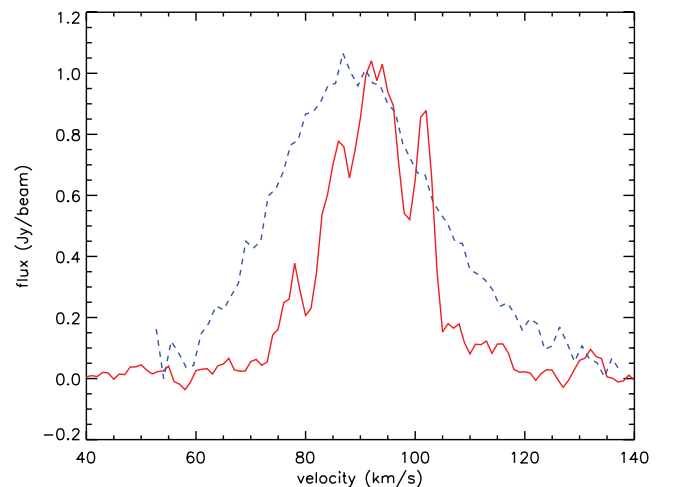


FIG. 2.—H53 α (dashed blue line) and H30 α (solid red line) in G28.20–0.04 N. The flux density of the H53 α line has been multiplied by 10.

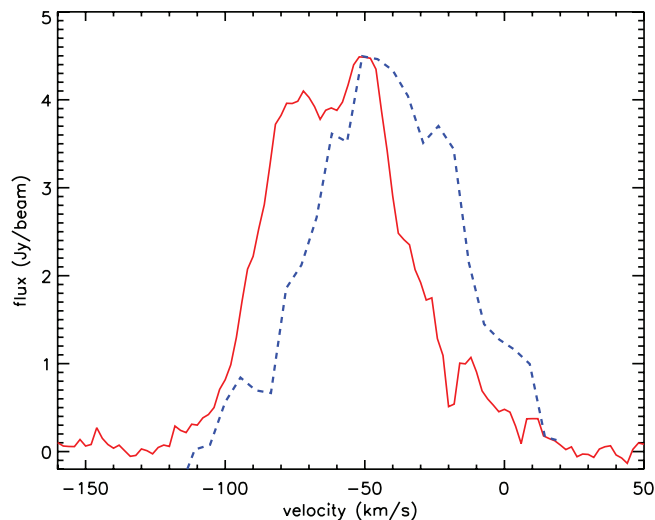


FIG. 3.—H30 α (solid red line) and H66 α (dashed blue line) in NGC 7538-IRS1. The flux density of the H66 α line has been multiplied by 190.

procedure assigns the line width to either the Gaussian or Lorentzian components primarily on the shape of the line wings where the profiles differ most strongly, but the signal-to-noise ratio is the weakest. Alternatively, one might estimate the FWHM directly from the three channels with the peak and half-power emission. However, because this estimate relies on single-channel measurements it is less reliable than a line-fitting procedure that uses measurements at all the channels across the line profile.

Several lines of evidence, discussed below in the paper, suggest that there are density variations within the H II regions. Because all the H II regions in our sample are unresolved, the measured electron density represents the average within the H II region. The size of the H II region within the beam (filling factor) does not affect this estimate of the average density, because the electron densities are determined from the line widths rather than the emission intensity. However, the unknown density structure of the H II region creates some uncertainty.

Aside from the systematic effects, the uncertainty in the average electron density is given by the standard propagation of errors, assuming the errors in the widths are independent. Uncertainties

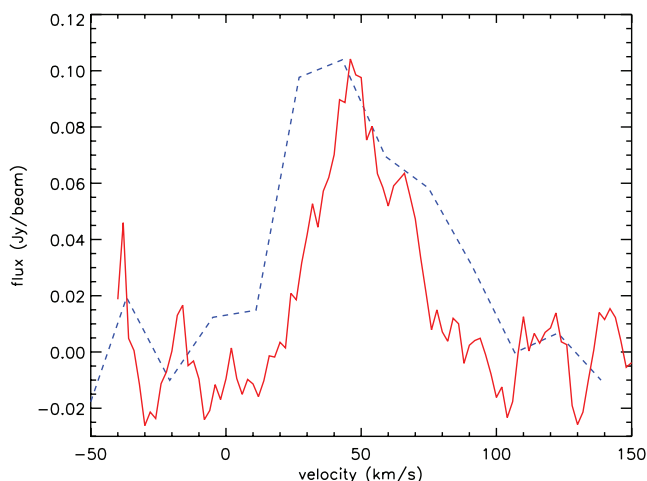


FIG. 4.—H76 α (dashed blue line) and H30 α (solid red line) in G45.07+0.13. The flux density of the H76 α line has been multiplied by 5.

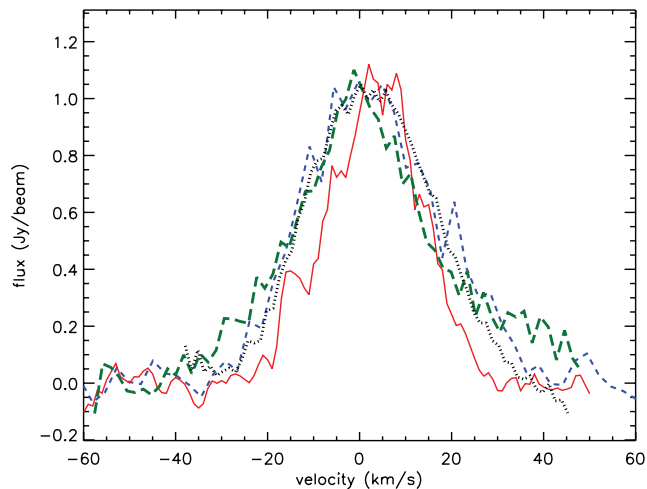


FIG. 5.—H92 α (long-dashed green line), H66 α (short-dashed blue line), H53 α (dotted black line), and H30 α (solid red line) in G10.6-0.04. The flux densities of the H92 α , H66 α , and H53 α lines have been multiplied by 115, 5.5, and 4.8, respectively.

in the electron densities are listed in Table 5 and for the line center velocities and widths in Table 4.

3.2. Electron Densities from the Radio Continuum

At the high densities in our H II regions, the centimeter continuum emission is optically thick to free-free emission. This can be determined from the formula (eq. [A.1b] in Mezger & Henderson 1967; eq. [10] in Keto 2003)

$$\tau_\nu = 8.235 \times 10^{-2} \left(\frac{T_e}{\text{K}} \right)^{-1.35} \left(\frac{\nu}{\text{GHz}} \right)^{-2.1} \left(\frac{\text{EM}}{\text{pc cm}^{-6}} \right), \quad (4)$$

where T_e is the electron temperature and the emission measure, $\text{EM} = \int_{-\infty}^{\infty} n_e^2 ds$, is the electron density squared times the path length. For a characteristic size of 0.01 pc, an H II region has an optical depth of unity at 22 GHz (1.3 cm) if the electron density is $4 \times 10^5 \text{ cm}^{-3}$. This means that the formulae for optically thin emission (e.g., Mezger & Henderson 1967) are not useful for the H II regions in our sample and probably not for small, high-density H II regions in general.

If the gas is optically thick to free-free emission and the electron density is estimated from the radio continuum by incorrectly assuming optically thin emission, then the derived electron density is just that density required to make the optical depth unity. This can be understood by a simple example. The radio free-free emission through a slab of uniform gas density and temperature is

$$S_\nu = 2kT_e(\nu^2/c^2)(1 - e^{-\tau_\nu})(\text{Jy/sr}). \quad (5)$$

The optically thin approximation amounts to replacing $[1 - \exp(-\tau_\nu)]$ by τ_ν so that

$$S_\nu \approx 2kT_e(\nu^2/c^2)\tau_\nu, \quad (6)$$

whereas in the optically thick limit,

$$S_\nu \approx 2kT_e(\nu^2/c^2). \quad (7)$$

TABLE 4
RECOMBINATION LINE DATA

Source	Continuum Peak (Jy beam ⁻¹)	Integrated		Line Peak (mJy beam ⁻¹)	1 σ (mJy beam ⁻¹)	Line Velocity ^a (km s ⁻¹)	1 σ (km s ⁻¹)	Line Width ^b (km s ⁻¹)	1 σ (km s ⁻¹)
		Intensity (Jy)	Quantum Number						
G10.6–0.4.....	0.017	3.14	92	8.1	0.2	0.6	0.5	37.5	1.2
	0.04 ^c	4.57	66	188.0	5.0	2.1	0.005	35.1	0.005
	2.1	6.0	53	219.0	4.9	2.2	0.005	31.8	0.01
	1.17	2.41	30	1040.0	28.5	3.4	0.3	24.5	0.8
G28.20–0.04 N	0.4	1.1	53	99.0	3.6	88.7	0.6	33.4	1.5
	0.56	0.72	30	930.0	22.0	92.5	0.2	20.9	0.6
G45.07+0.14	0.37	0.77	76	21.0	2.5	45.7	3.4	56.9	8.1
	0.08	0.17	30	92.0	10.2	49.4	1.8	33.2	4.2
W51e2.....	0.15	0.30	66	14.2	0.4	53.8	0.7	50.9	1.6
	0.17	2.3	53	42.0	1.1	59.5	0.3	32.5	1.2
	1.67	3.66	30	870.0	51.0	59.7	0.8	26.8	1.9
NGC 7538-IRS1	0.2	0.7	53	23.3	1.1	–41.8	1.0	61.0	4.1
	2.56	2.79	30	4450.0	58.0	–60.5	0.4	57.3	0.8

^a Line center velocity from Gaussian fit.

^b FWHM from Gaussian fit.

^c Keto 2002.

Thus, if the H II region is optically thick (eq. [7]) but τ_ν is derived assuming equation (6), then the derived value of the optical depth is 1, and the electron density derived from equation (4) is the density required to make $\tau_\nu = 1$. Thus at 22 GHz (1.3 cm), the electron density derived for an H II region with a size of 0.01 pc is never greater than about 10^5 cm^{-3} if the optically thin formulae are used—regardless of the true density. This underestimate also affects quantities derived from the electron density such as the number of ionizing photons required to balance recombinations, which in turn is often used to derive the spectral types of the exciting stars.

Formulae for spherical H II regions that have a density gradient such that the central part of the H II region is optically thick are derived in Keto (2003). However, these formulae require a specification of the size of the optically thick region.

3.3. The Correlation of Line Widths, Velocities, and Frequencies

As shown in Table 4, the line widths decrease with increasing frequency in all cases. This suggests the increasing importance of pressure broadening at lower frequencies. For sources with more than one centimeter RRL observed, the electron densities increase with the increasing frequency of the centimeter line used in the analysis. The one exception is the electron density calculated from the H66 α line in NGC 7538-IRS1. This line is very much wider and out of character with the other measurements in our sample. Aside from this one exception, the correlation of density with observing frequency indicates that the higher frequency lines are associated with higher density gas. The line center velocities also increase (redshift) with frequency, except for the lines of NGC 7538-IRS1.

TABLE 5
ELECTRON DENSITIES FROM LINE WIDTHS

Source	Quantum Number	Line Width (km s ⁻¹)	1 σ (km s ⁻¹)	n_e (cm ⁻³)	1 σ (cm ⁻³)
G10.6–0.4.....	92	37.5	1.2	9.1×10^4	7.3×10^3
	66	35.1 ^a	0.005	7.8×10^5	3.2×10^2
	53	31.8	0.01	2.5×10^6	3.2×10^3
G28.20–0.04 N	92	74.4 ^b	2.6	2.9×10^5	1.2×10^4
	53	33.4	1.5	4.1×10^6	4.3×10^5
G45.07+0.14	76	56.9 ^c	8.1	6.1×10^5	1.8×10^5
	66	42.3 ^d	2.3	6.9×10^5	1.6×10^5
W51e2.....	66	50.9	1.6	1.6×10^6	9.0×10^4
	53	32.5	1.2	2.0×10^6	4.0×10^5
NGC 7538-IRS1	66	180 ^e	...	1.0×10^7	...
	53	61.0	4.1	1.4×10^6	1.5×10^6

NOTE.—Electron density, n_e , required to produce the observed increase in the width of the centimeter RRL over the millimeter RRL by pressure broadening.

^a Keto 2002.

^b Sewilo et al. 2004.

^c Garay et al. 1986. The line width measured in our analysis of this data is larger than reported in the original reference (48.1 km s⁻¹).

^d Garay et al. 1985.

^e Gaume et al. 1995b.

TABLE 6
INTEGRATED INTENSITIES FROM PREVIOUS OBSERVATIONS

Source	Frequency (GHz)	Flux (Jy)	Beam (arcsec)	Reference
G10.6–0.4.....	23	2.4	0.1	Sollins & Ho 2005
	22.3	4.1	0.2 × 0.1	Keto & Wood 2006
	15	2.8	0.3	Ho & Haschick 1981
	15	2.6	0.3 × 0.2	Turner & Matthews 1984
	8.3	3.1	1.5 × 1.0	This paper
G28.20–0.04 N.....	5	1.7	1	Ho & Haschick 1981
	23.7	0.98	0.3 × 0.2	Sollins et al. 2005
	15	0.54	0.5	Kurtz et al. 1994
	8.4	0.30	0.9	Kurtz et al. 1994
G45.07+0.14.....	8.3	0.30	4.9 × 2.7	Sewilo et al. 2004
	345	2.71	3.0 × 4.0	Su et al. 2004
	98	1.04	2.6 × 2.4	Hunter et al. 1997
W51e2.....	147	3.7	2.0	Zhang et al. 1998
	88.2	1.23	6 × 5	Rudolph et al. 1990
	23.7	0.35	5 × 4	Rudolph et al. 1990
	14.7	0.26	4.1 × 3.9	Garay et al. 1985
	8.3	0.07	2.4	Mehring et al. 1994
	5.0	≤ 0.03	4.1	Mehring et al. 1994
	5.0	0.025	0.5	Rudolph et al. 1990

The combination of the two correlations, line center velocity with frequency and line width with frequency, was first noticed in W3(OH) by Berulis & Ershov (1983). Welch & Marr (1987) and Keto et al. (1995) interpreted the dual correlation as evidence for an accelerating flow within a density gradient (Guilloteau et al. 1983). A full explanation is given in Keto et al. (1995; see also Brocklehurst & Seaton 1972) and can be summarized as follows: the peak intensity of RRLs is proportional to the density squared and inversely proportional to the line width. Thus, the peak intensity of optically thin high-frequency lines with negligible pressure broadening is proportional to the density squared. The peak intensity of lower frequency lines is proportional to the first power of the density, since the pressure-broadened line width is itself proportional to density. Thus, in spatially unresolved observations of gas with a density gradient, the higher frequency RRLs are dominated by emission from the higher density gas, while the lower frequency RRLs include contributions from both high- and low-density gas. An observed difference in velocity between the high- and low-frequency lines thus indicates a difference in velocity between the high- and low-density gas.

The correlation of velocities and width with frequency therefore indicates that in these H II regions there is both a flow and a density gradient. The two are naturally related by the conservation of mass and the geometry of the flow. In general, if the flow is either outward and diverging or inward and converging, then conservation of mass requires that there be a density gradient except in the unique circumstance that the variation of the flow speed exactly cancels the geometric divergence or convergence.

4. CONTINUUM SPECTRAL INDICES

We determined the spectral energy distributions (SEDs) of the H II regions in our sample using our own millimeter and centimeter observations and data collected from the literature. We selected only those data with angular resolutions close to 1'', specifically excluding single-dish observations. Most of the data for NGC 7538-IRS1 and G45.07+0.14 are from Table 1 of Pratap et al. (1992) and Table 3 of Garay et al. (1986), respectively. The

rest of the observations are listed in Table 6. The original references for most of these data do not provide estimated uncertainties. However, the calibration of radio data is fairly standard. Many of the reported observations were made at the VLA that typically calibrated flux densities to better than 20% at 1.3 cm at the dates of the observations and much better at longer wavelengths. As noted in § 2, we estimate our SMA observations to be calibrated to better than 39%.

The SEDs are shown in Figures 6–10. Along with each observed SED, shown as crosses, the figures show two model SEDs as solid lines. One model SED is based on a single H II region

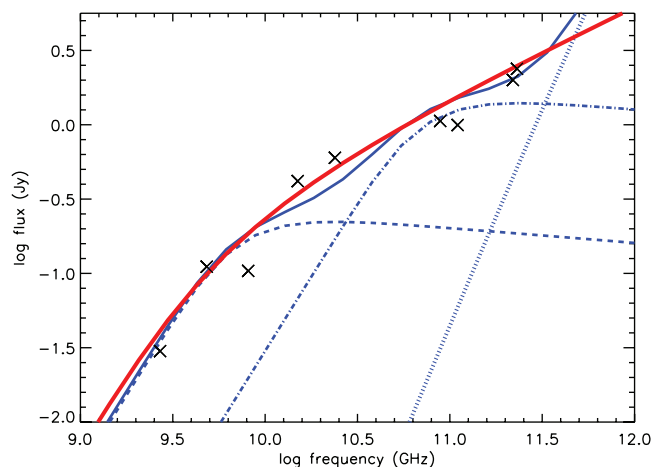


FIG. 6.—SED NGC 7538-IRS1. Data are from Table 1 of Pratap et al. (1992) with the addition of our 230 GHz SMA observation. The blue lines show a three-component model proposed by Pratap et al. (1992) consisting of two H II regions plus dust (*dotted line*). The dash-dotted line (of the smaller, higher density component) is shifted upward and to the right of the dashed line (of the larger, lower density component). The wavy solid blue line shows the sum of the three components. The red solid line that crosses smoothly through the waves of the three component model shows the SED of a single H II region with a power-law density gradient. See § 3 and Table 7.

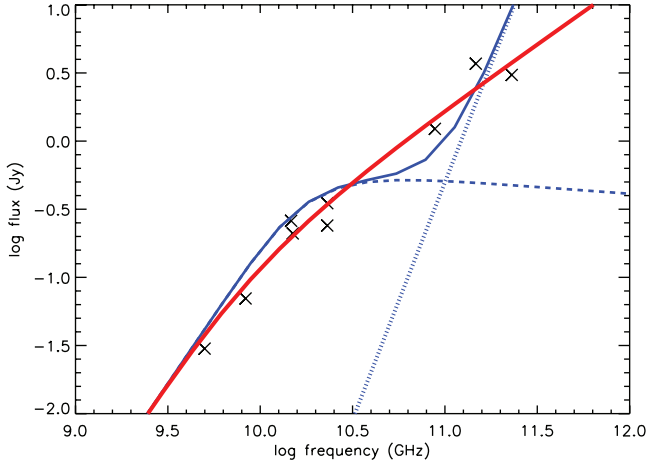


FIG. 7.—Measured flux densities of the W51e2 H II region (*crosses*). The blue dashed lines show a two-component model proposed by Rudolph et al. (1990) consisting of a uniform density H II region plus dust (*dotted line*). The solid red line is the SED predicted for an H II region with a density gradient ($n_e \propto r^{-1.3}$) and no significant dust emission. See § 3 and Table 7.

with a power-law density gradient. The continuum flux density for this model is calculated as in Keto (2003). The radio free-free emission of a spherical H II region seen as an unresolved source is

$$S_\nu = 4\pi k T_e \nu^2 / c^2 \int_0^{\theta_0} \theta (1 - e^{-\tau_\nu}) d\theta. \quad (8)$$

Here, θ is an angular coordinate on the plane of the sky, $\theta = (x^2 + y^2)^{1/2}/D$ with coordinate axes x and y centered on the H II region, $\theta_0 = R_0/D$, where R_0 is the radius of the H II region and D is the distance to the source. The free-free optical depth is given by equation (4). The model parameters for all sources are listed in Table 7.

The other model is an SED based on constant-density H II regions. The figures for NGC 7538-IRS1 and W51e2 show the SEDs from multicomponent models suggested by Pratap et al. (1992) and Rudolph et al. (1990). These are both based on constant-

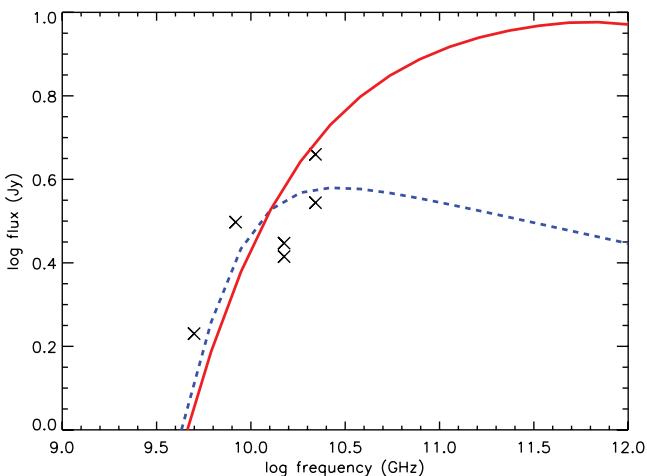


FIG. 8.—Measured flux densities of the G10.6–0.4 H II region (*crosses*). The blue dashed line is a model based on a uniform density H II region; the red line is a model based on an H II region with a density gradient.

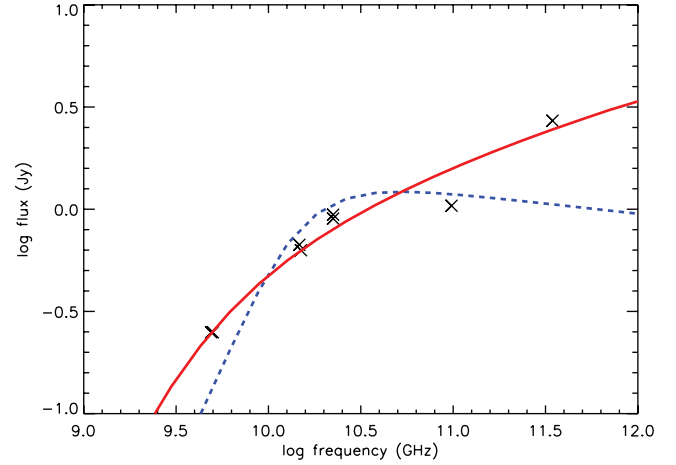


FIG. 9.—Continuum SED for G45.07+00.14. The crosses mark the observations; the blue dashed line is a model based on a uniform density H II region; the red line is a model based on an H II region with a density gradient.

density H II regions plus dust. The dust emission enters as (eq. [1] in Pratap et al. 1992)

$$S_\nu (\text{Jy}) = 52.36 M_\odot \left(\frac{0.2}{\lambda_{\text{mm}}} \right)^{\beta+3} \left[\exp \left(\frac{14.4}{\lambda_{\text{mm}} T_d} \right) - 1 \right]^{-1} D_{\text{kpc}}^{-2}, \quad (9)$$

where S_ν is the dust emission in Jy, M is the mass of the dusty gas in M_\odot , β is the spectral index of the dust emissivity, T_d is the dust temperature in degrees Kelvin, and D is the distance in kpc.

The multicomponent model for NGC 7538-IRS1 (Pratap et al. 1992) nicely illustrates how a density gradient within an H II region can stretch the transition between optically thick and thin frequencies resulting in an SED with an intermediate spectral index. In this model, there are two concentric spherical regions each of uniform but different densities. The smaller, higher density component produces an emission curve that is shifted upward and to the right of the curve for the larger, lower density component (Fig. 6). The emission from the two components

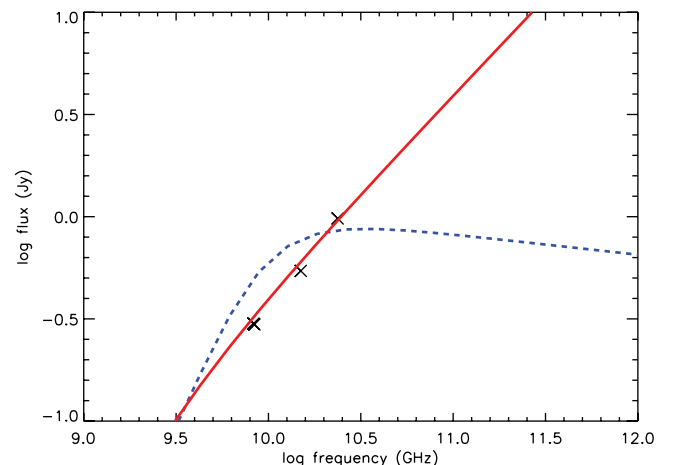


FIG. 10.—Continuum SED for G28.20–0.04. The crosses mark the observations; the blue dashed line is a model based on a uniform density H II region; the red line is a model based on an H II region with a density gradient.

TABLE 7
MODEL H II REGIONS FOR CONTINUUM SEDs

SOURCE	DISTANCE (kpc)	CONSTANT DENSITY		DENSITY GRADIENT		
		Radius (pc)	Density (cm^{-3})	Radius (pc)	Density (cm^{-3})	Exponent
G010.6–0.4.....	6.0	0.05	6.0×10^4	0.05	3.5×10^4	–1.4
G28.20–0.04 N.....	9.1	0.03	9.0×10^4	0.043	1.0×10^4	–2.5
G045.07+00.14.....	9.7	0.025	1.6×10^5	0.05	1.5×10^4	–1.7
W51e2 ^a	7.0	0.01	3.0×10^5	0.01	1.0×10^5	–2.5
NGC 7538-IRS1 ^b	3.5	0.02	2.7×10^6	0.08	2.7×10^6	–2.0
NGC 7538-IRS1 ^c	0.08	5.0×10^4

^a SED also includes a contribution from dust modeled as $4500 M_{\odot}$ of cold, dusty gas with a temperature of 100 K and a dust emissivity $\beta = 1.5$ from the model of Rudolph et al. 1990.

^b Constant density model with three components, two H II regions plus dust from the model of Pratap et al. 1992. The first H II component SED also includes a contribution from dust modeled as $53 M_{\odot}$ of cold, dusty gas with a temperature of 50 K and a dust emissivity $\beta = 1.0$.

^c Second component of constant density model.

combines to produce an SED of intermediate slope. An H II region with a continuous density gradient can be considered as the logical extension of this two-component model to many nested smaller and denser H II regions. Lugo et al. (2004) also model the NGC 7538-IRS1 H II region with a density gradient that they suggest is due to a wind off a photoevaporating disk.

The SED modeling combined with the recombination line measurements shows that dust is not a significant contributor to the continuum emission measured at high angular resolution from these sources (see also Kurtz 2005; DePree et al. 1998, 2000). Consider W51e2 as an example. As seen in Figure 7, the H II region can be modeled with uniform, low-density ionized gas, with the 147 and 230 GHz emission arising from dust (Rudolph et al. 1990). Figure 7 shows that with this approach, the free-free continuum emission at 230 GHz would be about a factor of 10 below the observed emission. However, the line-to-continuum ratio should be approximately one at this frequency (Gordon & Sorochenko 2002). Hence, if the free-free continuum were this low, the H30 α recombination line would also have a much lower flux density—so low that the line would not be detected in our observations. Stated another way, the recombination line emission cannot be 10 times greater than the free-free continuum emission at this frequency. Therefore, most of the continuum emission observed by the interferometer at 231.901 GHz must be free-free; hence, the electron density must be higher, and a density gradient is required.

The high-frequency emission observed in large beams (20''–30'') around these bright H II regions certainly arises from dust. Again, take W51e2 as an example. Jaffe et al. (1984) report a flux density of $1200 \text{ Jy beam}^{-1}$ at 750 GHz and 40'' angular resolution. We assume, as in the model of Rudolph et al. (1990), that this emission is from cool dust in the large-scale molecular cloud surrounding the H II region. Because the dust is cool (50–100 K), a large mass of dust is required ($4500 M_{\odot}$; Rudolph et al. 1990) to produce the observed 750 GHz flux density. While the emission from this dust is also sufficient to produce the 90 and 230 GHz flux density that is observed by interferometers, the cool dust is not the source of this emission, because it is not possible that this large mass of cool dusty gas is within the spatial scale defined by the arcsecond angular resolution of the interferometers. However, the ionized gas is sufficiently hot (10^4 K) that only a small mass ($0.01 M_{\odot}$), consistent with the mass of the H II regions, is

required to produce the 90–230 GHz flux density. Similar considerations apply to the multicomponent models of other H II regions, for example, the model discussed earlier for NGC 7538-IRS1 (Pratap et al. 1992).

On a spatial scale similar to that of HCH II and UCH II regions, continuum emission from dust has been observed by the SMA in the nearby (1.7 kpc) massive star-forming region NGC 6334 by Hunter et al. (2006). The dusty clumps of arcsecond scale in NGC 6334 have continuum emission on the order of 1 Jy. Scaled to the distance of W51, the dust in such clumps would be a minor contributor (60 mJy) to the continuum emission. Thus, high-angular resolution observations of dusty clumps in NGC 6334 are consistent with the interpretation of negligible dust contribution to the emission observed at high angular resolution in more distant bright H II regions.

5. DISCUSSION

The observations suggest that pressure broadening of the centimeter RRLs is important in small H II regions. This contradicts the interpretation of some previous studies. In particular, on the basis of electron densities calculated by assuming constant gas density and optically thin emission, Gaume et al. (1995b) and DePree et al. (1997, 2005) have suggested that the electron densities in NGC 7538-IRS1, W49, and Sgr B2 are too low to cause significant pressure broadening in the H66 α line. However, the multifrequency RRL observations suggest that the electron density in NGC 7538-IRS1 is 2 orders of magnitude greater than the 10^5 cm^{-3} derived by Gaume et al. (1995b) and sufficient to cause significant pressure broadening. Jaffe & Martín-Pintado (1999) report observations of millimeter RRLs of several sources, including G10.6–0.4 and NGC 7538-IRS1. They concluded that the RRL widths are not due to pressure broadening, because the observed widths of different recombination lines do not scale as the fourth power of the frequency. Their conclusion was based on a comparison of observations with different angular resolutions. It has been demonstrated that low-angular resolution observations may suffer confusion from more extended, lower density gas (Simpson 1973a, 1973b; Gulyaev & Sorochenko 1974; Smirnov et al. 1984; Gordon & Sorochenko 2002). We concur with Gaume et al. (1995b), DePree et al. (1997, 2005), and Jaffe & Martín-Pintado (1999) that broadening due to gas motions is significant, but we find that pressure broadening is as well.

The intermediate SEDs of small H II regions imply a density gradient as would arise from a divergence or convergence in the flow of ionized gas in an H II region. Other interpretations are possible. Franco et al. (2000), Kurtz & Franco (2002), and Kim & Koo (2002) suggested that the various densities are due to the hierarchical structure of the molecular cloud prior to its ionization by a massive star. The intermediate SEDs can also be created by density variations other than gradients. Ignace & Churchwell (2004) suggested that an H II region is actually an ensemble of differently sized clumps, each of uniform but different density. One problem with these models of pre-existing structure or clumps is that their survival time is approximately their sound crossing time. This timescale seems impossibly short if the high-density clumps are substructures within an HCH II ($t_c \leq 1000$ yr for $R < 0.01$ pc).

The interpretation of density gradients and resulting high electron densities in small H II regions also contradicts the interpretation of significant dust emission in a number of other studies. For example, Rudolph et al. (1990), Pratap et al. (1992), Testi et al. (2000), Schilke et al. (1990), and Beuther et al. (2004, 2006) model the small H II regions, W51e2, NGC 7538-IRS1, G9.62+0.19-F, and Orion-KL-SMA1, respectively, with low- and constant-density gas and assume that dust makes up the emission at high frequencies. Testi et al. (2000) also provide an alternative model with a stellar wind rather than dust to supply the high-frequency emission. These models with low and constant density have difficulty in explaining the broad RRL line widths. If the density is low, then the widths must be due to dynamical broadening created by a supersonic flow. However, in the context of the dynamics of H II regions, a constant density is not generally consistent with supersonic flows. In general, a strong density gradient is required to create the strong pressure gradient needed to drive the flow.

6. CONCLUSIONS

1. The radio recombination line widths increase with decreasing frequency in all cases. This indicates the greater importance of pressure broadening at lower frequencies.

2. The electron densities calculated by comparison of centimeter recombination lines with the H30 α millimeter line increase with increasing frequency of the centimeter line. This suggests that the higher frequency lines are generated in denser gas and suggest that density gradients exist in small H II regions.

3. Supersonic line widths are observed in the H30 α RRL. This line is at a frequency high enough that pressure broadening is negligible provided that the density of the emitting gas is less than 10^8 cm $^{-3}$. The large line widths suggest the presence of supersonic motions within the H II regions.

4. The electron densities in HCH II and UCH II regions are generally high enough that the gas is optically thick at centimeter wavelengths. This means that electron densities cannot be calculated from radio continuum observations using formulae that assume optically thin emission. Instead, formulae appropriate for partially optically thick emission must be used.

5. At high frequencies (≥ 100 GHz) and high angular resolution ($\sim 1''$), the observed continuum emission is mostly free-free emission and not from dust. Comparisons based on high-frequency observations with different beam sizes can lead to erroneous conclusions. High-frequency emission at low angular resolution ($\geq 10''$) is probably from dust, but associated with the large-scale, overlying molecular cloud.

S.K acknowledges support from UNAM, DGAPA project IN106107.

REFERENCES

- Afflerbach, A., Churchwell, E., Hofner, P., & Kurtz, S. 1994, *ApJ*, 437, 697
 Altenhoff, W. J., Strittmatter, P. A., & Wendker, H. J. 1981, *A&A*, 93, 48
 Berulis, I. I., & Ershov, A. A. 1983, *Soviet Astron. Lett.*, 9, 341
 Beuther, H., et al. 2004, *ApJ*, 616, L31
 ———. 2006, *ApJ*, 636, 323
 Brocklehurst, M., & Seaton, M. J. 1972, *MNRAS*, 157, 179
 DePree, C. G., Gaume, R. A., Goss, W. M., & Claussen, M. J. 1995, *ApJ*, 451, 284
 ———. 1996, *ApJ*, 464, 788
 DePree, C. G., Goss, W. M., & Gaume, R. A. 1998, *ApJ*, 500, 847
 DePree, C. G., Goss, W. M., Palmer, P., & Rubin, R. 1994, *ApJ*, 428, 670
 DePree, C. G., Mehringer, D. M., & Goss, W. M. 1997, *ApJ*, 482, 307
 DePree, C. G., Wilner, D. J., Deblasio, J., Mercer, A. J., & Davis, L. E. 2005, *ApJ*, 624, L101
 DePree, C. G., Wilner, D. J., Goss, W. M., Welch, W. J., & McGrath, E. 2000, *ApJ*, 540, 308
 DePree, C. G., Wilner, D. J., Mercer, A. J., Davis, L. E., Goss, W. M., & Kurtz, S. 2004, *ApJ*, 600, 286
 Franco, J., Kurtz, S., Hofner, P., Testi, L., Guillermo, G.-S., & Martos, M. 2000, *ApJ*, 542, L143
 Garay, G., Reid, M. J., & Moran, J. M. 1985, *ApJ*, 289, 681
 Garay, G., Rodriguez, L. F., & van Gorkom, J. H. 1986, *ApJ*, 309, 553
 Gaume, R. A., Claussen, M. J., DePree, C. G., Goss, W. M., & Mehringer, D. M. 1995a, *ApJ*, 449, 663
 Gaume, R. A., Goss, W. M., Dickel, H. R., Wilson, T. L., & Johnston, K. 1995b, *ApJ*, 438, 776
 Giveon, U., Becker, R. H., Helfand, D. J., & White, R. L. 2005a, *AJ*, 129, 348
 ———. 2005b, *AJ*, 130, 156
 Gordon, M. A., & Sorooshenko, P. N. 2002, *Radio Recombination Lines: Their Physics and Astronomical Applications* (Dordrecht: Kluwer)
 Griem, H. R. 1974, *Spectral Line Broadening by Plasmas* (New York: Academic)
 Guilloteau, S., Stier, M. T., & Downes, D. 1983, *A&A*, 126, 10
 Gulyaev, S. A., & Sorooshenko, R. L. 1974, *Astron. Zh.*, 51, 1237
 Ho, P., & Haschick, A. D. 1981, *ApJ*, 248, 622
 Hofner, P., Kurtz, S., Churchwell, E., Walmsley, C., & Cesaroni, R. 1996, *ApJ*, 460, 359
 Hunter, T. R., Brogan, C. L., Megeath, S. T., Menten, K. M., Beuther, H., & Thorwirth, S. 2006, *ApJ*, 649, 888
 Hunter, T. R., Phillips, T. G., & Menten, K. M. 1997, *ApJ*, 478, 283
 Ignace, R., & Churchwell, E. 2004, *ApJ*, 610, 351
 Jaffe, D. T., Becklin, E. E., & Hildebrand, R. H. 1984, *ApJ*, 279, L51
 Jaffe, D. T., & Martín-Pintado, J. 1999, *ApJ*, 520, 162
 Johnson, C. O., DePree, C. G., & Goss, W. M. 1998, *ApJ*, 500, 302
 Keto, E. 2002, *ApJ*, 568, 754
 ———. 2003, *ApJ*, 599, 1196
 Keto, E., Welch, W., Reid, M., & Ho, P. T. P. 1995, *ApJ*, 444, 765
 Keto, E., & Wood, K. 2006, *ApJ*, 637, 850
 Kim, K.-T., & Koo, B.-C. 2002, in *RevMexAA Conf. Ser. 12, Ionized Gaseous Nebulae*, ed. W. Henney et al. (México, D.F.: Instituto de Astronomía), 27
 Kurtz, S. 2000, in *RevMexAA Conf. Ser. 9, Astrophysical Plasmas: Codes, Models, and Observations*, ed. J. Arthur, N. Brickhouse, & J. Franco (México, D.F.: Instituto de Astronomía), 169
 ———. 2005, in *IAU Symp. 227, Massive Star Birth: A Crossroads of Astrophysics*, ed. R. Cesaroni et al. (Cambridge: Cambridge Univ. Press), 111
 Kurtz, S., Churchwell, E., & Wood, D. 1994, *ApJS*, 91, 659
 Kurtz, S., & Franco, J. 2002, in *RevMexAA Conf. Ser. 12, Ionized Gaseous Nebulae*, ed. W. Henney et al. (México, D.F.: Instituto de Astronomía), 16
 Lugo, J., Lizano, S., & Garay, G. 2004, *ApJ*, 614, 807
 Mehringer, D. 1994, *ApJS*, 91, 713
 Mezger, P. G., & Henderson, A. P. 1967, *ApJ*, 147, 471
 Olivero, J. J., & Longbothum, R. L. 1977, *J. Quant. Spectrosc. Radiat. Transfer*, 17, 233
 Pratap, P., Snyder, L. E., & Batrla, W. 1992, *ApJ*, 387, 241
 Rudolph, A., Welch, W. J., Palmer, P., & Dubrulle, B. 1990, *ApJ*, 363, 528
 Schilke, P., Mauersberger, R., Walmsley, C. M., & Wilson, T. J. 1990, *A&A*, 227, 220
 Sewilo, M., Churchwell, E., Kurtz, S., Goss, W. M., & Hofner, P. 2004, *ApJ*, 605, 285

- Simpson, J. P. 1973a, *Ap&SS*, 20, 187
———. 1973b, *PASP*, 85, 479
Sollins, P., & Ho, P. T. P. 2005, *ApJ*, 630, 987
Sollins, P., Zhang, Q., Keto, E., & Ho, P. T.P 2005, *ApJ*, 631, 399
Smirnov, G. T., Sorochenko, R. L., & Pankonin, V. 1984, *A&A*, 135, 116
Su, Y.-N., et al. 2004, *ApJ*, 616, L39
Testi, L., Hofner, P., Kurtz, S., & Rupen, M. 2000, *A&A*, 359, L5
Tieftrunk, A. R., Gaume, R. A., Claussen, M. J., Wilson, T. L., & Johnston, K. J. 1997, *A&A*, 318, 931
Turner, B. E., & Matthews, H. E. 1984, *ApJ*, 277, 164
Walsh, A. J., Burton, M. G., Hyland, A. R., & Robinson, G. 1998, *MNRAS*, 301, 640
Welch, Wm. J., & Marr, J. 1987, *ApJ*, 317, L21
Wilson, T. L., Boboltz, D. A., Gaume, R. A., & Megeath, S. T. 2003, *ApJ*, 597, 434
Wood, D. O. S., Wood, & Churchwell, E. 1989, *ApJS*, 69, 831
Zhang, Q., Ho, P. T. P., & Ohashi, H. 1998, *ApJ*, 494, 636
Zijlstra, A. A., Pottasch, S. R., Engels, D., Roelfsema, P. R., te Lintel Hekkert, P., & Umana, G. 1990, *MNRAS*, 246, 217